J Appl Electrochem (2007) 37:1203–1217
DOI 10.1007/s10800-007-9364-7

ORIGINAL PAPER

Models of Hypochlorite production in electrochemical reactors with plate and porous anodes

C. Y. Cheng · G. H. Kelsall

Received: 24 February 2007 / Revised: 15 May 2007 / Accepted: 2 July 2007 / Published online: 4 August 2007

Abstract Pseudo two-dimensional finite element models were developed to predict the hypochlorite (chloric(I)) ($HOCl + OCl^-$) production by electrolysis of near-neutral aqueous sodium chloride solution, in reactors with (a) an anode and cathode in the form of plates, and (b) a lead dioxide-coated graphite felt anode and titanium plate cathode. The model was used to investigate the feasibility of using a porous anode to achieve high single pass conversions in oxidising chloride ions. For the model reactor with planar anode, the effects of diffusion, migration and convection on the mass transport of the reacting species were considered, whereas with the porous anode, a supporting electrolyte (Na_2SO_4) was notionally present to eliminate the migrational contribution to reactant transport. For an electrolyte flow rate of 10^{-6} m^3 s^{-1} (Re = 10 for plate electrodes, Re_{porous} = 0.76 for porous anode), a cell voltage of 3.0 V and an inlet NaCl of 100 mol m^{-3}, the single-pass conversion of Cl^- was predicted to increase from 0.45 for the reactor with a planar anode to 0.81 for the reactor with a porous anode. For the same operating conditions, the overall current efficiency was also predicted to increase from 0.71 to 0.77 by replacing the plate with the porous anode.

Keywords Hypochlorite · Chloric(I) · Chloride · Modelling · Porous electrode

Notation

A	Specific surface area of porous electrode (m^2 m^{-3})
C_i	Concentration of species i (mol m^{-3})
$C_{i,in}$	Inlet concentration of species i (mol m^{-3})
D_i	Diffusion coefficient of species i (m^2 s^{-1})
d	Distance between the planar anode and cathode (m)
d_f	Fibre diameter (m)
d_h	Hydraulic diameter of felt fibre (m)
E_k	Equilibrium electrode potential of reaction k versus reference electrode (SHE) (V)
F	Faraday constant (C mol^{-1})
j_k	Current density of reaction k (A m^{-2})
j_L	Limiting current density (A m^{-2})
j_0	Exchange current density (A m^{-2})
k	Standard heterogeneous rate constant coefficient (m s^{-1})
k_m	Mass transport rate coefficient (m s^{-1})
K	Equilibrium constant (mol^{-1} dm^3)
N_i	Superficial flux of species i (mol m^{-2} s^{-1})
n	Number of electrons involved in a reaction (–)
R	Universal gas constant (J mol^{-1} K^{-1})
Re	Reynolds number for reactor with planar electrodes (vd/ν) (–)
Re_{porous}	Reynolds number for porous electrode ($v_{eff}d_h/\nu$)
r_k	Rate of homogeneous reaction k (mol m^3 s^{-1})
t	Time (s)
T	Temperature (K)
U_{cell}	Cell voltage (V)
u_i	Mobility of ion i in an electric field (z_iFD_i/RT) (m^2 V^{-1} s^{-1})
V	Linear electrolyte velocity (m s^{-1})
v_{eff}	Solution velocity in the empty cross-section area (m s^{-1})
z_i	Number of charge on species i (–)
i	Subscript i refers to reacting species (–)
k	Subscript k refers to reactions (–)

C. Y. Cheng · G. H. Kelsall (✉)
Department of Chemical Engineering, Imperial College London, London SW7 2AZ, UK
e-mail: g.kelsall@imperial.ac.uk

s	Subscript s refers to solid phase (–)
l	Subscript l refers to liquid phase (–)
a	Subscript a refers to anode properties (–)
c	Subscript c refers to cathode properties (–)
α	Transfer coefficient (–)
β_a	Tafel coefficient, i.e. $(1-\alpha)nF/(RT)$ (V^{-1})
β_c	Tafel coefficient, i.e. $\alpha\ nF/(RT)$ (V^{-1})
ε	Voidage of the graphite felt electrode (–)
δ	Diffusion layer thickness (m)
κ_s	Effective solid phase conductivity within graphite felt electrode (S m^{-1})
κ_l	Effective liquid phase conductivity within graphite felt electrode (S m^{-1})
$\kappa_{l,0}$	Pure liquid phase (electrolyte) conductivity (S m^{-1})
κ	Permeability of porous material (m^2)
η	Overpotential of reaction (V)
υ	Stoichiometric coefficient (–)
ν	Kinematic viscosity ($m^2\ s^{-1}$)
$\Phi_{overall}$	Overall current efficiency (–)
Φ_c	Potential at feeder cathode electrode (V)
Φ_a	Potential at feeder anode electrode (V)

1 Introduction

The uses of hypochlorite (chloric(I)) ($HOCl + OCl^-$) include chemical oxidations, disinfection of drinking water, sewage, process equipment in food and beverage industries, and also sterilisation of injection water in oil wells and of cooling water to prevent fouling of heat transfer surfaces in power stations. Due to the extreme hazard of storing and transporting liquid chlorine, aqueous absorption of which produces hypochlorite species ($HOCl + OCl^-$), local electrogeneration of hypochlorite is expected to become mandatory in the future.

There is extensive literature on modelling and experimental studies of hypochlorite (choric(I)) and chlorate production, which have also been the subject of reviews [1–3]. Ibl and Vogt [1] developed kinetic models to predict the concentration profiles of the species involved in the anode reaction layer in hypochlorite/chlorate electrogeneration. The formation of hypochlorite in either hypochlorite or chlorate electrochemical reactors involves the initial formation of chlorine, which is hydrolysed in a reaction layer at the anode. The hypochlorite concentration profile within the reaction layer leads to some of the hypochlorite diffusing back to the electrode and being further oxidised to chlorate. Ibl and Landolt [4, 5] investigated anodic ClO_3^- formation in dilute NaCl and concentrated NaCl solutions on graphite anodes, at which the rate of ClO_3^- formation was determined to be proportional to OCl^- concentration and the mass transport of $HOCl/OCl^-$ towards the anode was the rate-determining step. Robertson et al. [6] determined experimentally that the rate of electro-oxidation of $HOCl/OCl^-$ on dimensionally stable anodes (DSAs—Ti/RuO_2) was independent of electrolyte flow rate and hence, kinetically controlled and its rate on DSA was lower than that on graphite or platinised titanium, as the anodic overpotentials required for Cl_2 evolution on DSAs are much lower than those on graphite or platinised titanium.

Current efficiency losses due to hypochlorite reduction at cathodes have been investigated experimentally and theoretically. At the low potentials of hydrogen-evolving cathodes, the rate of hypochlorite reduction was found to be proportional to the concentration of OCl^- and the reaction rate was limited by the diffusion of OCl^- to the surface of the cathode, and correlated to the electrolyte velocity [2, 6, 7]. Rudolf et al. [8] predicted that migrational transport away from the cathode decreased the flux of OCl^- by up to 50 %, relative to the diffusion flux alone of OCl^- towards the cathode in a stagnant electrolyte layer.

The objective of the work reported here was to investigate theoretically the performance of graphite felt, electrodeposited with lead dioxide [9], as a flow-by anode to enable high single pass conversions of chloride to hypochlorite. This was achieved using finite element models of such a reactor with homogeneous reactions coupled to the electrode reactions, but for initial model development and for comparison purposes, a reactor with a plate anode and cathode pair, as shown schematically in Fig. 1, was also modelled.

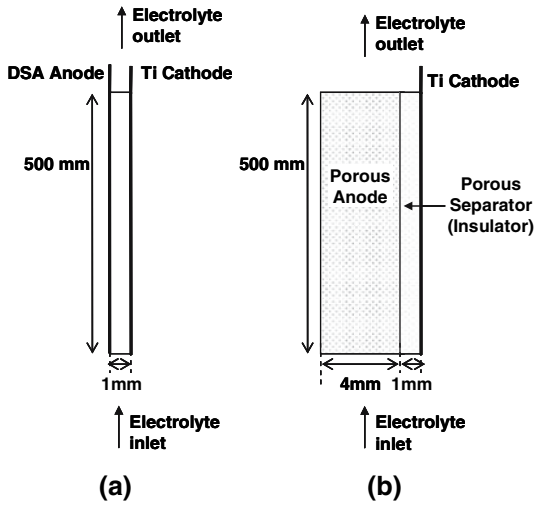

Fig. 1 Schematic diagram for flow-by reactors with (**a**) plate electrodes and (**b**) porous anode and plate cathode

2 Chemistry and electrochemistry of chlorine–water systems

Electrolysis of near-neutral aqueous chloride solutions in an undivided electrochemical reactor involves the following primary reactions [10] with equilibrium equations calculated for 298 K:

Anode:

$$Cl_2(aq) + 2e^- \leftarrow 2Cl^- \tag{1}$$

$$E_{Cl_2/Cl^-}(SHE)/V = 1.396 + 0.0296 \log [Cl_{2(aq)}]\gamma_{Cl_2} - 0.0592 \log [Cl^-]\gamma_{Cl^-} \tag{2}$$

where square bracket represents concentration in mol dm^{-3} and γ_i represents the activity coefficient of species i; for dilute solutions, the activity coefficients were assumed to be close to unity. In the model calculations all equilibrium potentials were defined using concentrations at the surface of the electrodes.

Cathode:

$$2H_2O + 2e^- \rightarrow H_2 + 2OH^- \tag{3}$$

$$E_{H_2O/H_2}(SHE)/V = -0.828 - 0.0592 \log [OH^-]\gamma_{OH^-} - 0.0296 \log P_{H_2} \tag{4}$$

The rate of reaction (1) may be kinetically or transport controlled, depending on the applied current density, chloride ion concentration, and the prevailing hydrodynamic conditions, which may also depend on the rate of anodic gas evolution [11]; hence, these parameters also control the current efficiency of reaction (1).

In the model described in this paper a sufficient overpotential ($\eta_{Cl_2} = \Phi_a - \phi - E_{Cl_2/Cl^-}$) was applied to drive reaction (1) into mixed kinetic and mass-transport control to ensure high conversion of Cl^-; the current density (j_{Cl_2}) can then be estimated by the Butler–Volmer equation, neglecting the component due to the rate of the back reaction, as the overpotential was sufficiently high as to involve minimal error:

$$j_{Cl_2} = j_{0,Cl_2}\left\{\left(\frac{C_{Cl^-,s}}{C_{Cl^-,b}}\right)\exp\left[\beta_{Cl_2}\left(\Phi_a - \phi - E_{Cl_2/Cl^-}\right)\right]\right\} \tag{5}$$

where ϕ represents the liquid phase potential relative to the same reference electrode as used to define the equilibrium potential.

For the electro-oxidation of Cl^- on two-dimensional Ti/RuO_2 plate or mesh ('DSAs') anodes, as used industrially, an exchange current density (j_{0,Cl_2}) of 1 A m^{-2} [3, 12] and a Tafel slope of 30 mV $decade^{-1}$ [13], were used, as reported in the literature. The Tafel slope was estimated as ca. 90 mV $decade^{-1}$ for Cl^- oxidation on a planar Ti/PbO_2 anode in 500 mol m^{-3} NaCl at pH 6.7–8.1 and 296–298 K, although the behaviour was dependent on the conditions used for anodic deposition of PbO_2. As discussed below further oxidation of the chloric(I) product in batch recycle systems and the analytical difficulties of defining the resulting solution compositions complicate the determination of kinetic parameters.

The current density of hydrogen evolution (reaction (3)) (j_{H_2}) was under kinetic control, which can be estimated by:

$$j_{H_2} = j_{H_2,0} \cdot \exp\left[\beta_{H_2}\left(\Phi_c - \phi - E_{H_2O/H_2}\right)\right] \tag{6}$$

An exchange current density ($j_{H_2,0}$) of 0.01 A m^{-2} and a Tafel slope of 140 mV $decade^{-1}$ were used in the models, as these values have been reported in literature for hydrogen evolution on titanium electrodes in 6 M NaOH at 298 K [14].

If the local concentration of dissolved chlorine exceeds its solubility then supersaturation will drive the formation of bubbles:

$$Cl_2(aq) \rightleftarrows Cl_2(g) \tag{7}$$

$$\log[Cl_2] = -1.26 + \log P_{Cl_2} \tag{8}$$

However, aqueous chlorine may also form trichloride ions as indicated in reaction (9); their concentration would be insignificant in the models described below but are important in reactors producing chlorate and chlorine from more concentrated (>1 M) chloride solutions:

$$Cl_2 + Cl^- \rightleftarrows Cl_3^- \tag{9}$$

$$\log\left\{\left[Cl_3^-\right]/[Cl_2]\right\} = -0.66 + \log[Cl^-] \tag{10}$$

As chlorine diffuses away from the anode it hydrolyses and disproportionates by the reaction:

$$Cl_{2(aq)} + H_2O \rightleftarrows HOCl + Cl^- + H^+ \tag{11}$$

$$\log\left\{[HOCl]/\left[Cl_{2(aq)}\right]\right\} = pH - 3.33 - \log[Cl^-] \tag{12}$$

According to Spalding [15], reaction (11) is reversible for pH < 3 and irreversible for pH > 3, with an apparent forward rate constant of 20.9 s^{-1} at 298 K. Due to the production of protons by O_2 evolution (reaction (18)), the pH close to the anode is predicted to be less than 3 and so within the anode diffusion boundary layer, the rate of Cl_2 hydrolysis (r_1 mol dm^{-3} s^{-1}) was calculated by:

$$r_1 = k_{1f}\left[Cl_{2(aq)}\right] - k_{1b}[HOCl][Cl^-][H^+] \tag{13}$$

and elsewhere in the electrolyte by:

$$r_1 = k_{1f}\left[Cl_{2(aq)}\right] \quad (14)$$

The forward (k_{1f}) and backward (k_{1b}) rate constants for hydrolysis of chlorine determined experimentally with a solution of 0.5 mol dm^{-3} ionic strength at 298 K are 22.3 s^{-1} and 2.14×10^4 (mol $dm^{-3})^{-2}$ s^{-1}, respectively; hence the equilibrium constant (K_1) is 1.04×10^{-3} (mol $dm^{-3})^2$ [16].

If the bulk solution pH is neutral or alkaline, the chloric(I) acid formed will dissociate to its ions:

$$HOCl \rightleftarrows H^+ + OCl^- \quad (15)$$

$$\log\{[OCl^-]/[HOCl]\} = pH - 7.55 \quad (16)$$

$$r_2 = k_{2f}[HOCl] - k_{2b}[OCl^-][H^+] \quad (17)$$

The equilibrium constant for the dissociation of chloric(I) acid (K_2) calculated by thermodynamic data at 298 K is 2.81×10^{-8} [10]. As the kinetics of such deprotonation reactions are very fast in general, it was assumed to be at equilibrium and the backward rate constant (k_{2b}) was chosen to be 1×10^8 (mol $dm^{-3})^{-1}$ s^{-1}. The forward rate coefficient (k_{2f}) was calculated from ($k_{2b} \times K_2$). With this value reaction (15) was close to equilibrium and the effect of further increasing k_{2b} was shown to be insignificant.

Figure 2 shows a speciation diagram, summarising the homogeneous chemistry of 'active chlorine' (i.e. Cl_2 (aq) + Cl_3^-, + HOCl + OCl^-), which indicates the uncertainties in the gas/liquid equilibria involving Cl_2O and HClO (g) [17], the predicted partial pressure of the latter being unrealistically high.

The following loss reactions also occur to an extent depending on the conditions:

Anode loss reaction:

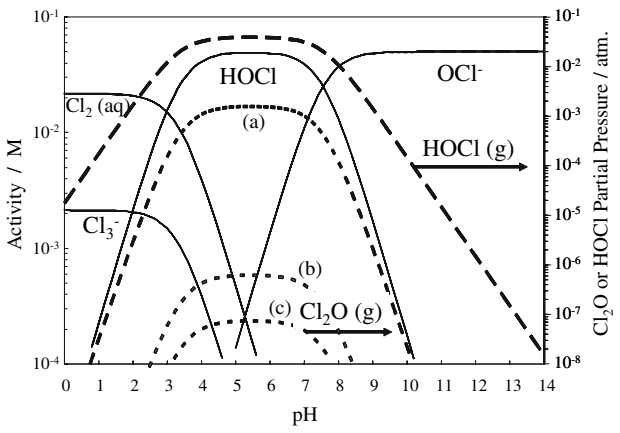

Fig. 2 Activity–pH diagram for chlorine–water system at 298 K for $P(Cl_2)$ at 1 atm. Predicted Cl_2O (g) partial pressure using data from: (**a**) Roth [16]; (**b**) Ourisson [16]; (**c**) [19]

$$O_2\,(g) + 4H^+ + 4e^- \leftarrow 2H_2O \quad (18)$$

$$E_{O_2/H_2O}(SHE)/V = 1.229 - 0.0592 \cdot pH + 0.0148 \cdot \log(P_{O_2}) \quad (19)$$

$$j_{O_2} = j_{0,O_2} \cdot \exp\left[\beta_{O_2}\left(\Phi_a - \phi - E_{O_2/H_2O}\right)\right] \quad (20)$$

For the kinetically controlled partial current density of O_2 evolution (j_{O_2}) (reaction (18)), an exchange current density ($j_{O2,0}$) of 10^{-6} A m^{-2} and transfer coefficient (α_{O_2}) of 0.5 ($\beta_{O_2} = \frac{\alpha_{O_2} n_{O_2} F}{RT}$) were used, as reported in the chlorate production model developed by Byrne [3], but the value of $j_{O_2,0}$ is of the same magnitude as reported in [18].

As the hydrolysis reaction (11) and the loss reaction (18) produce protons, the pH in the anode diffusion layer (thickness X_D) decreases to values at which chlorine is the primary product (Fig. 2) and its (fast) hydrolysis occurs within a reaction layer (thickness X_R), if the bulk electrolyte is near neutral or slightly alkaline. Some of the resulting HOCl diffuses out to the bulk electrolyte, depending on its bulk concentration, and some diffuses back to the anode, at which it is oxidised further, allegedly [19] by the overall reaction:

$$2ClO_3^- + 4Cl^- + 1.5O_2 + 12H^+ + 6e^- \leftarrow 6HOCl + 3H_2O \quad (21)$$

More probably, a series of one-electron reactions are involved in Cl^{I} oxidising to Cl^{V}, the first of which would produce Cl^{II}; data were reported in the most recent critically assessed thermodynamic data source [20] only for $Cl^{II}O$ (g) species:

$$Cl^{II}O(g) + H^+ + e^- \leftarrow HOCl^{I} \quad (22)$$

$$E_{ClO(g)/HOCl}\,(SHE)/V = 1.845 - 0.0592\,pH + 0.0296\,\log P_{ClO} - 0.0296\,\log(HOCl) \quad (23)$$

However, presumably Cl^{II} species adsorbed on the electrode could also be formed as intermediate species in the overall two electron oxidation:

$$Cl^{III}O_2^- + 3H^+ + 2e^- \leftarrow HOCl^{I} + H_2O \quad (24)$$

$$E_{ClO_2^-/HOCl}\,(SHE)/V = 1.7323 - 0.0887\,pH + 0.0296\,\log\left(ClO_2^-\right) - 0.0296\,\log(HOCl) \quad (25)$$

or

$$Cl^{III}O_2^- + 2H^+ + 2e^- \leftarrow Cl^{I}O^- + H_2O \quad (26)$$

$$E_{ClO_2^-/ClO}\,(SHE)/V = 1.5089 - 0.0592\,pH + 0.0296\,\log\left(ClO_2^-\right) - 0.0296\,\log(OCl^-) \quad (27)$$

This could be followed by:

$$Cl^{IV}O_2(aq) + e^- \leftarrow Cl^{III}O_2^- \tag{28}$$

$$E_{ClO_2/ClO_2^-}(SHE)/V = 1.0406 + 0.0592\ \log(ClO_2) - 0.0592\ \log\left(ClO_2^-\right) \tag{29}$$

the predicted aqueous solubility of gaseous chlorine dioxide being high at 298 K:

$$\log(ClO_2(aq)) = 0.51 + \log P(ClO_2(g)) \tag{30}$$

Finally:

$$Cl^{V}O_3^- + 2H^+ + e^- \leftarrow Cl^{IV}O_2(aq) + H_2O \tag{31}$$

$$E_{ClO_3^-/ClO_2}(SHE)/V = 1.2051 - 0.1183\,pH + 0.0592\ \log\left(ClO_3^-\right) - 0.0592\ \log(ClO_2) \tag{32}$$

Although there is disagreement in the literature [2, 4, 5, 13, 19, 20] about the rate and route of ClO_3^- formation by oxidation of HOCl (reaction (21)), the consensus is that its rate is of minor importance on DSAs under conditions typical of those used in hypochlorite reactors. As a result it is reasonable to omit this reaction from the model for the parallel plate reactor with a DSA anode.

However, experiments with Ti/PbO_2 anodes suggested that the rate of HOCl oxidation may be significant on PbO_2 (coated graphite felt), for which electrode potentials at constant current would be significantly greater than at a DSA. The equilibrium potentials for the reaction sequence (24)/(26), (28) and (31) at near neutral pH are less positive than that for chlorine evolution, according to Eq. 2, so chloric(I) oxidation at potentials less positive than those required for chloride oxidation would be expected. If HOCl oxidation were to be included in the model, more H^+ would be produced at the anode and the pH in the anode diffusion layer would be lower. If the rate of HOCl oxidation was assumed to be proportional to the concentration of HOCl/OCl^-, its partial current density would increase with anode height and hence, current efficiencies for chloric(I) formation would decrease with anode height. Due to the complexity of the reaction mechanism, lack of reproducibility of the kinetics of Cl^- oxidation on Ti/PbO_2 and the lack of reliable kinetic data on that or any other anode material, HOCl oxidation was not included in the porous anode model, for which results are presented below.

At the hydrogen-evolving cathodes reaction (3) results in a high local pH (ca. 12–13, depending on current densities and mass transport rates), so that active chlorine species diffusing into the cathode diffusion layer from the bulk solution are converted to OCl^- ions, and are reduced under transport control by the reaction:

Cathode loss reaction:

$$OCl^- + H_2O + 2e^- \Leftrightarrow Cl^- + 2OH^- \tag{33}$$

$$E_{OCl^-/Cl^-}(SHE)/V = 1.718 - 0.0591\,pH + 0.0296\ \log\{[OCl^-]/[Cl^-]\} \tag{34}$$

Due to the very large overpotential for reaction (33) at a hydrogen-evolving cathode, the reduction of OCl^- is normally under total mass transport control and the concentration of OCl^- at the surface of cathode is zero. Its current density can be calculated by the flux of OCl^- (N_{OCl^-}) towards cathode; the contribution from diffusion and migration to mass transport are both significant, but migration opposes the diffusional flux, since hypochlorite anions migrate from cathode to anode in the electric field. The migration effect was predicted to decrease the flux of OCl^- towards the cathode by up to 50% with respect to the flux due to diffusion alone [8].

$$j_{OCl^-} = n_{OCl^-}FN_{OCl^-} \tag{35}$$

$$N_{OCl^-} = -D_{OCl^-}\frac{dC_{OCl^-}}{dx} - u_{OCl^-}C_{OCl^-}\frac{d\phi}{dx} \tag{36}$$

The combination of loss reactions (21) and (33) limits the maximum hypochlorite concentration achievable in hypochlorite reactors to ca. 0.1 M. [10, 19]. In addition, further homogeneous loss reactions, such as (chemical) chlorate formation, may occur in the bulk solution, but can be assumed to have insignificant rates at ambient temperatures:

$$2HOCl + OCl^- \rightarrow ClO_3^- + 2Cl^- + 2H^+ \tag{37}$$

$$2ClO^- \rightarrow 2Cl^- + O_2 \tag{38}$$

$$ClO^- + H_2 \rightarrow H_2O + Cl^- \tag{39}$$

Lastly, the concentration of protons and hydroxide ions in the bulk electrolyte were maintained at equilibrium by the water dissociation reaction:

$$H_2O \Leftrightarrow H^+ + OH^- \tag{40}$$

$$r_{H_2O} = k_{H_2O,f}[H_2O] - k_{H_2O,b}[OH^-][H^+] \tag{41}$$

The value of the backward rate constant ($k_{H_2O,b}$) was chosen to be 1.4×10^6 (mol $dm^{-3})^{-1}$ s^{-1}, as further increase had insignificant effect on the model predictions. The forward rate coefficient ($k_{H_2O,f}$) was calculated from ($k_{H_2O,b} \times K_{H_2O}$), where ($K_{H_2O}$) is 10^{-14}.

3 Model Development

In order to investigate the feasibility of using a PbO_2 coated graphite felt as an anode to increase Cl^- conversion

and hypochlorite production, models for flow-by reactors with parallel plate electrodes were developed to predict the performance of existing reactors, together with a reactor with a PbO_2-coated graphite felt as anode and a plate electrode as cathode. Both model reactors were operated under constant cell voltage with the electrolyte flowing upwards, as shown in Fig. 1. Since convection was constant and dominated exclusively in the vertical direction, diffusion and migration terms could be neglected in that direction, so pseudo two-dimensional models were sufficient to predict the behaviour of the reactors. The species considered in the reaction system were: Na^+, Cl^-, H^+, OH^-, OCl^-, $Cl_{2(aq)}$, O_2, H_2 and HOCl. A summary of the diffusion coefficients is shown in Table 1 [21, 22]. The reactions included in the models were: (1), (3), (11), (15), (18), (33) and (40). The schematic diagram of the model geometry for the reactor with (a) plate electrodes and (b) porous anode and plate cathode is shown in Fig. 3.

3.1 Reactor with plate electrodes

As gas evolution at both electrodes dominates the hydrodynamic behaviour of the reactor, rather than solving the Navier–Stokes equation, the model geometry of the reactor with plate electrodes was divided into three regions: the anode diffusion boundary layer (R1), the bulk electrolyte (R2) and the cathode diffusion boundary layer (R3), as shown in Fig. 3a. The bulk electrolyte was assumed to be well-mixed.

Table 1 A summary of diffusion coefficients

Diffusion coefficients at 298 K		
Species	Diffusion coefficient, D_i ($m^2\ s^{-1}$)	Reference
Na^+	1.334×10^{-9}	[21]
Cl^-	2.032×10^{-9}	[21]
$Cl_{2(aq)}$	1.83×10^{-9}	[22]
H^+	9.312×10^{-9}	[21]
OH^-	5.260×10^{-9}	[21]
OCl^-	1.10×10^{-9}	[22]
HOCl	1.28×10^{-9}	[22]

The thickness of cathode and anode diffusion boundary layer (δ_c, δ_a) can be estimated by:

$$\delta_c = \frac{D_{OCl^-}}{k_{m,c}}; \quad \delta_a = \frac{D_{Cl^-}}{k_{m,a}} \tag{42}$$

The mass transport was assumed to be controlled by convective diffusion and the mass transfer coefficient at the hydrogen-evolving cathode ($k_{m,c}$) can be estimated from the correlation:

$$k_{m,c} = a_{constant}\left(1.3 + 1.7v^{0.71}\right)10^{\left[-5+0.24\left(\frac{j_{H_2}}{1000}\right)^{0.38}\right]} \tag{43}$$

where $a_{constant}$ is a factor depending on the nature of surface of the electrode, with a value of 1 for aged electrode and a value of 1.5 for a fresh electrode [11].

It was assumed that the empirical Eq. 43 could also be used to estimate the mass transfer coefficient at the oxygen-evolving anode ($k_{m,a}$), allowing for the O_2 bubble evolution rate being half that of the corresponding hydrogen-evolving cathode:

$$k_{m,a} = a_{constant}\left(1.3 + 1.7V^{0.71}\right)10^{\left[-5+0.24\left(\frac{0.5j_{O_2}}{1000}\right)^{0.38}\right]} \tag{44}$$

As an estimate, the average current density was assumed to be 1000 A m^{-2}. The cathode efficiency was assumed to be 1 and the (mean) cathode diffusion boundary layer estimated by Eqs. 42 and 43 was 50 μm. Assuming 5 % of the anode current density is lost to O_2 evolution, the anode diffusion boundary layer estimated by Eqs 42 and 44 was 125 μm, whereas if chlorine were evolved as bubbles rather than being hydrolysed by reaction (11), then the anode diffusion layer thickness would be 80 μm. As an initial estimate, the thicknesses of both the anode and cathode diffusion boundary layers were assumed to be 100 μm in this model.

The electrolyte velocity was assumed to be uniform within the bulk electrolyte (v_{ave}). The no-slip condition was

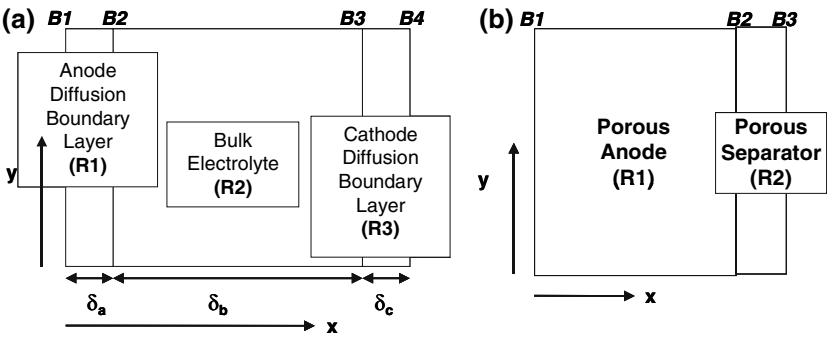

Fig. 3 Schematic diagram of the model geometries for the reactors with (**a**) plate electrodes and (**b**) porous anode and plate cathode

applicable at the surface of electrodes, i.e. where $v = 0$, and parabolic flow within anode and cathode boundary layers was assumed. The hydrodynamics of a reactor with bubbles-evolving electrodes is complicated and could not be predicted accurately by the method proposed here. The thicknesses of the anode and cathode boundary layers vary with the height of the electrodes, as the current density changes. The velocity profile proposed here was used as an estimate only.

At steady-state ($dC_i/dt = 0$), the concentrations in the model are governed by the material balance:

$$\frac{\partial C_i}{\partial t} = -\nabla \cdot N_i + \sum_k \upsilon_{ik} r_k = 0 \tag{45}$$

and electroneutrality:

$$\sum_i z_i C_i = 0 \tag{46}$$

In the pseudo two-dimensional model the flux (N_i) was described by the Nernst–Planck equation:

$$N_i = \left(-D_i \frac{dC_i}{dx} - u_i C_i \frac{d\phi}{dx}\right) + vC_i \tag{47}$$

So Eq. 45 becomes:

$$\frac{d}{dx}\left(-D_i \frac{dC_i}{dx} - u_i C_i \frac{d\phi}{dx}\right) + v\frac{dC_i}{dy} = \sum_k \upsilon_{ik} r_k \tag{48}$$

The boundary condition at the surface of the anode and cathode is given by:

$$N_i = \sum_k \frac{\upsilon_{ik} j_k}{n_k F} \tag{49}$$

At the reactor inlet the concentration was specified as:

$$C_i = C_{i,\text{in}} \tag{50}$$

At the outlet the convective flux is dominant:

$$N_i = vC_i \tag{51}$$

The equations were implemented in COMSOL Multiphysics software and solved by the finite element method.

3.2 Reactor with porous anode and plate cathode

The permeability of the porous anode (PbO_2-coated graphite felt) was ca. 10^{-9} m^2 [23]. Choosing a porous separator (insulator) with similar structure as the porous anode can minimise the electrolyte by-passing the porous anode. Porous structures encourage even distribution of the flow of electrolyte and hence, the velocity profile was assumed to be uniform in this model, the geometry of which was divided into two sub-domains: porous anode (R1) and porous separator (R2), as shown in Fig. 3b.

As it would be complicated to include migrational transport within the pores of the electrode, a supporting electrolyte (500 mol m^{-3} Na_2SO_4) was notionally added to the model solution, to eliminate the migration contribution to transport rates. This would suffice for the purpose of investigating the feasibility of using the graphite felt as the anode for hypochlorite production.

As the migrational contribution to the overall mass transport of Cl^- was insignificant in the presence of excess supporting electrolyte, the current density for the electro-oxidation of Cl^- ions in the porous electrode can be modified to:

$$j_{Cl_2} = \frac{j_{0,Cl_2} \exp\left(\beta_{Cl_2}\left(\phi_s - \phi_l - E_{Cl_2/Cl^-}\right)\right)}{1 + \left(\frac{j_{0,Cl_2}}{j_{L,Cl_2}}\right) \exp\left(\beta_{Cl_2}\left(\phi_s - \phi_l - E_{Cl_2/Cl^-}\right)\right)} \tag{52}$$

where j_{L,Cl_2} is the mass transport limiting current density (by diffusion alone), estimated by:

$$j_{Cl_2,L} = n_{Cl_2} F k_m C_{Cl^-,b} \tag{53}$$

where $C_{Cl^-,b}$ is the concentration of Cl^- in the bulk of the pores of the graphite felt electrode and k_m is the mass transfer coefficient within the pores, estimated from [24]:

$$k_m = 3.19\left(\frac{D_{Cl^-}}{d_h}\right)\left(\frac{v_{\text{eff}} d_h}{\upsilon}\right)^{0.69}; \quad v_{\text{eff}} = \frac{v}{\varepsilon}; \qquad d_h = \frac{4\varepsilon}{(4/d_f)(1-\varepsilon)} \tag{54}$$

Within the porous anode, the solid phase potential (ϕ_s) obeys Ohm's law and is related to the current density at the solid/liquid interface by:

$$-\kappa_s \frac{d^2\phi_s}{dx^2} = j_a a \tag{55}$$

j_a is the total current density at the solid/liquid interface in the anode, i.e. $j_{Cl_2} + j_{O_2}$, a is the specific surface area of the graphite felt, which was assumed to be 10^4 m^2 m^{-3} [23] and κ_s is the effective solid phase conductivity, calculated from Bruggeman's equation:

$$\kappa_s = \kappa_{PbO_2}(1-\varepsilon)^{1.5} \tag{56}$$

where ε is the porosity of the porous anode, for which a value of 0.95 was assumed (Le Carbone Lorraine RVC 2003).

At the feeder anode boundary the solid phase potential was defined by:

$$\phi_s = \Phi_a \tag{57}$$

At the interface between porous electrode and bulk electrolyte all current is carried in the liquid phase and so:

$$\frac{d\phi_s}{dx} = 0 \tag{58}$$

As a result of the presence of excess supporting electrolyte, the liquid phase potential (ϕ_l) also obeys Ohm's law. Within the porous anode, it is governed by:

$$\kappa_l \frac{d^2\phi_l}{dx^2} = j_a a \tag{59}$$

and in the porous separator, by:

$$\kappa_l \frac{d^2\phi_l}{dx^2} = 0 \tag{60}$$

κ_l is the effective liquid phase conductivity calculated by Bruggeman's equation:

$$\kappa_l = \kappa_{l,0}\varepsilon^{1.5} \tag{61}$$

where

$$\kappa_{l,0} = \sum_i \frac{z_i^2 F^2 C_i D_i}{RT} \tag{62}$$

assuming that dilute solution theory is applicable.

At the feeder anode and cathode all current is carried in the solid phase and so:

$$\frac{d\phi_l}{dx} = 0 \tag{63}$$

In the presence of excess supporting electrolyte the migration contribution to overall mass transfer rates was negligible, the diffusion coefficient was modified within the porous anode, and the material balance became:

$$\frac{d}{dx}\left(-\varepsilon D_i \frac{dC_i}{dx}\right) + v\frac{dC_i}{dy} = \sum_k \upsilon_{ik} r_k + \sum_k \frac{\upsilon_{ik} j_k a}{n_k F} \tag{64}$$

and in the remaining electrolyte:

$$\frac{d}{dx}\left(-\varepsilon D_i \frac{dC_i}{dx}\right) + v\frac{dC_i}{dy} = \sum_k \upsilon_{ik} r_k \tag{65}$$

As the surface area of the graphite felt anode was much greater than that of the anode feeder, most of the electrochemical reaction occurred within the porous anode. In order to simplify the problem the flux of reactants from the anode feeder caused by electrochemical reactions was assumed to be insignificant and so, at the feeder anode:

$$N_i = 0 \tag{66}$$

and at the cathode the flux is governed by:

$$N_i = \sum_k \frac{\upsilon_{ik} j_k}{n_k F} \tag{67}$$

At the reactor inlet the concentration was specified:

$$C_i = C_{i,\text{in}} \tag{68}$$

At the outlet the flux was dominated by convection:

$$N_i = vC_i \tag{69}$$

The equations were implemented and solved by the finite element method in COMSOL Multiphysics software.

4 Model predictions and discussion

The concentration and partial current density distributions within the reactors, together with conversions and current efficiencies, were predicted by the models.

4.1 Concentration and pH distributions

Figure 4 shows the predicted concentrations of (a) Cl^-, (b) $Cl_{2(aq)}$, (c) HOCl within the anode boundary layer, and (d) OCl^- within the cathode boundary layer; Fig. 5 shows the predicted pH within (a) the anode diffusion boundary layer and (b) the cathode diffusion boundary layer, for the reactor with plate electrodes, operating at an applied cell voltage of 3.0 V with an average current density of 220 A m^{-2}, an electrolyte volumetric flow rate of 10^{-6} m^3 s^{-1} (equivalent to a linear velocity of 10^{-2} m s^{-1}, Re = 10) and an inlet NaCl concentration of 100 mol m^{-3}.

The concentration of Cl^- decreased non-linearly from its bulk electrolyte value towards the surface of the anode (Fig. 4a). The non-linearity was caused by the contribution of migration to mass transfer and by chemical reactions in the boundary layer. The bulk concentration of Cl^- was predicted to decrease from 100 mol m^{-3} at the inlet of the reactor to 55 mol m^{-3} at the reactor's outlet, achieving a single-pass Cl^- conversion of 0.45. The Cl^- concentration at the surface of the anode was predicted to decrease rapidly along the height of the reactor. However, the surface Cl^- concentration indicates that Cl^- oxidation by reaction (1) was not totally mass transport controlled under this specific set of operating conditions.

$Cl_{2(aq)}$ was produced by the electro-oxidation of Cl^- at the anode. As Cl^- concentrations decreased with height of the reactor, the production rate of $Cl_{2(aq)}$ also decreased with height (Fig. 4b). $Cl_{2(aq)}$ concentration decreased with

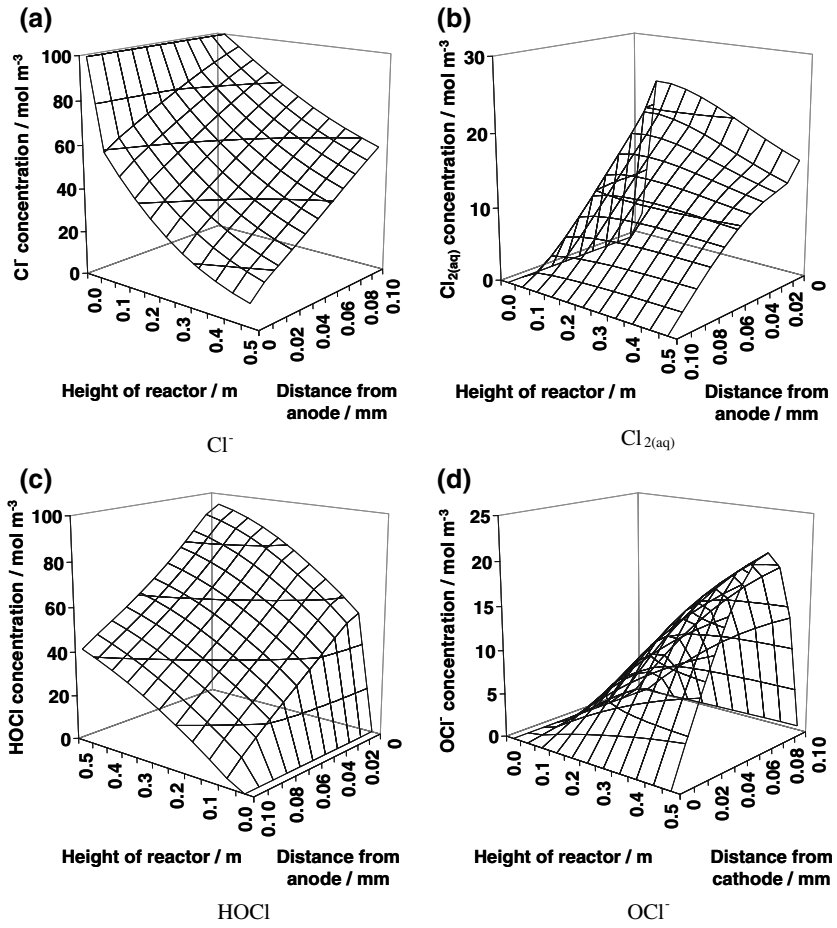

Fig. 4 Predicted concentrations of (**a**) Cl^-, (**b**) $Cl_{2(aq)}$, (**c**) HOCl within the anode boundary layer, and (**d**) OCl^- within the cathode boundary layer; for the reactor with plate electrodes operating at a cell voltage of 3.0 V, an electrolyte flow rate of 10^{-6} m^3 s^{-1} and an inlet NaCl concentration of 100 mol m^{-3}

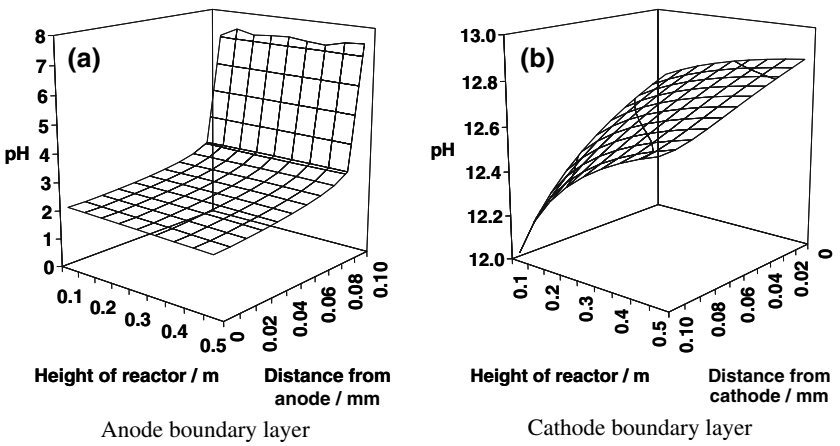

Fig. 5 Predicted pH within (**a**) anode diffusion boundary layer and (**b**) cathode diffusion boundary layer; for the reactor with plate electrodes operating at a cell voltage of 3.0 V, an electrolyte flow rate of 10^{-6} m^3 s^{-1} and an inlet NaCl concentration of 100 mol m^{-3}

distance from the anode as it was converted into HOCl, Cl^- and H^+ by hydrolysis (reaction (11)). In the vicinity of the anode the hydrolysis of $Cl_{2(aq)}$ was reversible, since a value of pH 2 was predicted (Fig. 5a), as H^+ was produced by O_2 evolution (reaction (18)) at the anode. The H^+ concentration decreased with distance away from the anode surface, as H^+ was neutralised by OH^- produced at the cathode and then transported to the bulk electrolyte. The pH increased to 7 towards the bulk electrolyte, where hydrolysis of $Cl_{2(aq)}$ was predicted to be irreversible. The bulk concentration of $Cl_{2(aq)}$ was negligible, which supported reports in the literature that, due to fast hydrolysis, all $Cl_{2(aq)}$ was converted to hypochlorite species [19].

Figure 4c shows the predicted concentration of HOCl within the anode boundary layer. Hydrolysis of $Cl_{2(aq)}$ produced HOCl (reaction (11)), which then dissociated to

form H^+ and OCl^- ions (reaction (15)). Due to the low pH, the HOCl concentration was in equilibrium with $Cl_{2(aq)}$, Cl^- and H^+ within the anode boundary layer. Its concentration was greatest close to the anode, where the $Cl_{2(aq)}$ concentration was highest, and HOCl was transferred towards the bulk electrolyte by diffusion, but undergoing fast dissociation. In the bulk solution, the HOCl concentration was in equilibrium with the concentrations of OCl^- and H^+. Had its further oxidation by the reaction sequence (24)/(26), (28) and (31) been allowed within the model, then its concentration at the anode surface would have been depleted.

OH^- was produced at the cathode due to both H_2 evolution and the reduction of OCl^-, so the cathode boundary layer pH was 12–13, as shown in Fig. 5b. Hence, as predicted in Fig. 2, in the cathode boundary layer all active chlorine species were converted to OCl^- ions, which were then reduced at the cathode by reaction (33), resulting in the peak in concentration shown in Fig. 4d. Due to large overpotentials for the reduction of OCl^-, its rate was under total mass transport control and the OCl^- concentration at the cathode surface was zero for the entire height of cathode. However, since hypochlorite anions migrated from cathode to anode in the electric field, migration opposed the diffusional flux and hence the flux of OCl^- towards the cathode was smaller than that due to diffusion alone, as implied by the migrational and diffusional flux data in Fig. 6a and b, respectively.

Figure 7 shows the predicted concentration profiles of (a) Cl^-, (b) $Cl_{2(aq)}$, (c) HOCl within the porous anode, and (d) OCl^- close to the cathode (region R2 in Fig. 3b), while Fig. 8 shows the predicted pH within (a) the porous anode and (b) close to the cathode. Both sets of graphs were for the reactor with porous anode and plate cathode, at a cell voltage of 3.0 V, with an average current density of 307 A m^{-2}, and an electrolyte volumetric flow rate of 10^{-6} m^3 s^{-1} (equivalent to a linear velocity of 0.002 m s^{-1}) (Re_{porous} = 0.76) and an inlet NaCl concentration of 100 mol m^{-3}.

The concentration represents those in the bulk of the pores of the anode, not on the surface of the porous anode. The Cl^- concentrations were predicted to decrease from the inlet to the outlet of the reactor, with outlet Cl^- concentrations <10 mol m^{-3} within the porous anode, except in the region (0.5 mm) close to the porous anode/porous separator interface (Fig. 7a). As Cl^- was not consumed within the inter-electrode gap, its concentration was higher in the porous separator region (>4 mm from feeder). In the region between 0 and 3.5 mm from the anode feeder, the Cl^- concentration decreased with distance from the feeder; as that distance increased, the potential difference between the solid and liquid phase increased and hence, overpotentials and current densities for oxidation of Cl^- ions increased.

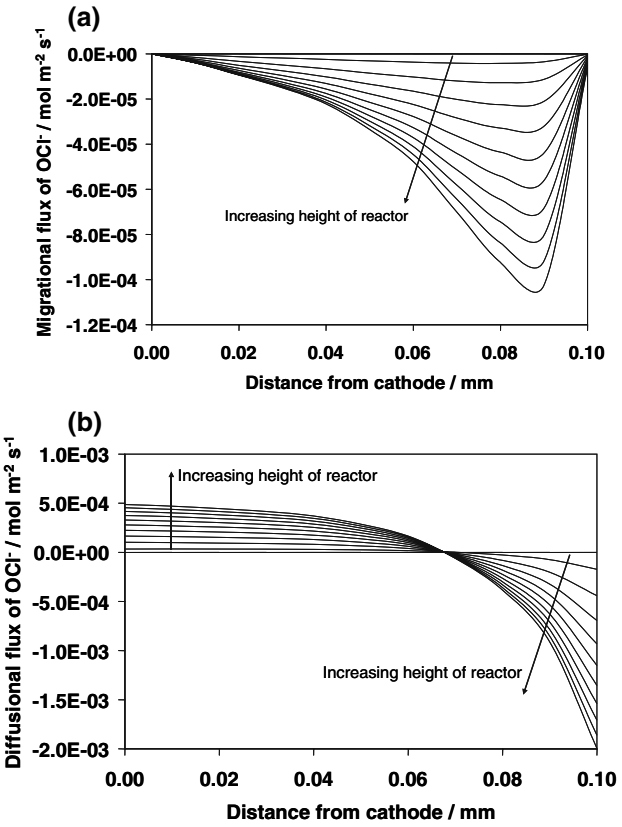

Fig. 6 Predicted (**a**) migrational flux and (**b**) diffusional flux of OCl^- within the cathode boundary layer; for the reactor with plate electrodes operating at a cell voltage of 3.0 V, an electrolyte flow rate of 10^{-6} m^3 s^{-1} and an inlet NaCl concentration of 100 mol m^{-3}

As Cl^- concentrations and, hence, current densities for oxidation of Cl^- were greatest at the reactor inlet, $Cl_{2(aq)}$ concentrations increased at a faster rate closer to the reactor inlet (Fig. 7b). Since H^+ was produced by O_2 evolution within the porous anode, pH < 2.1 was predicted within the entire porous anode (Fig. 8a) and the hydrolysis of $Cl_{2(aq)}$ was reversible. As $Cl_{2(aq)}$ species were hydrolysed to form HOCl, HOCl concentrations increased (Fig. 7c) with anode height.

A value of pH 14 was predicted for the electrolyte close to the cathode (Fig. 8b), due to OH^- produced by H_2 evolution at the cathode, so active chlorine species from the bulk solution were converted entirely to OCl^- ions, as predicted in Fig. 2. The concentration of OCl^- increased with HOCl concentration along the height of the reactor (Fig. 7d), but OCl^- ions were reduced at the cathode under total mass transport control.

4.2 Current densities

Figure 9 shows the predicted current density profiles of Cl^- oxidation (j_{Cl_2}), O_2 evolution (j_{O_2}) and total anode

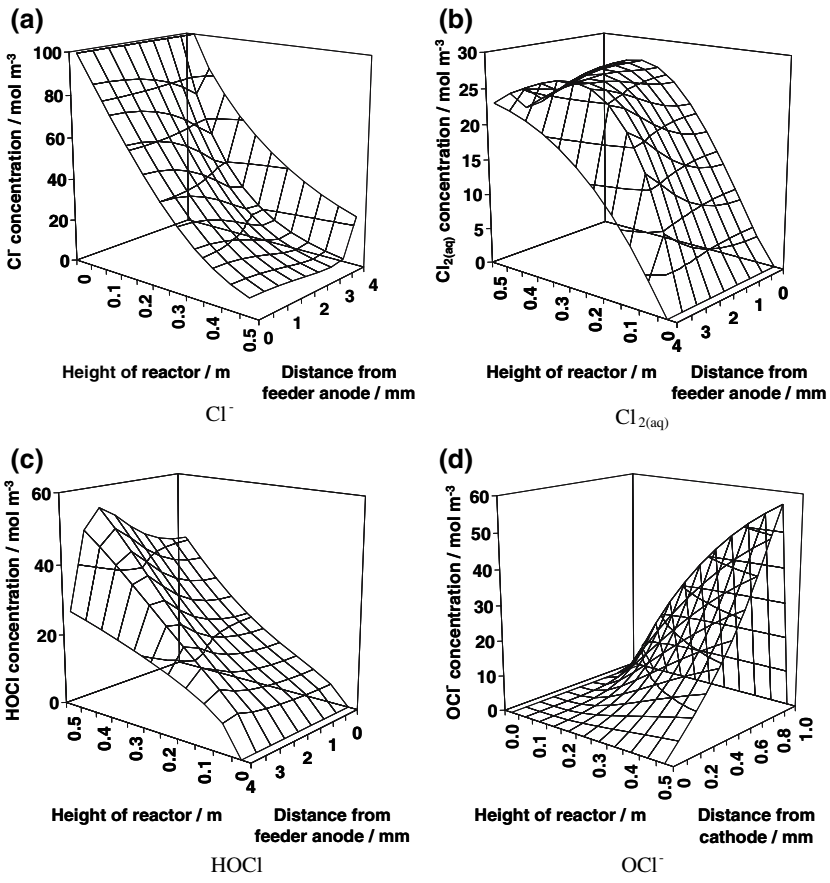

Fig. 7 Predicted concentrations of (**a**) Cl^-, (**b**) $Cl_{2(aq)}$, (**c**) HOCl within the porous anode, and (**d**) OCl^- close to the cathode (region R2 in Fig. 3b); for the reactor with porous anode and plate cathode operating at a cell voltage of 3.0 V, an electrolyte flow rate of 10^{-6} m^3 s^{-1} and an inlet NaCl concentration of 100 mol m^{-3}

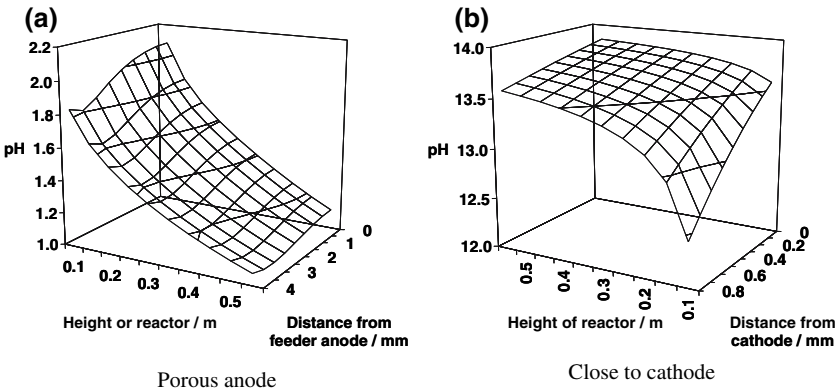

Fig. 8 Predicted pH within (**a**) porous anode and (**b**) close to cathode (region R2 in Fig. 3b); for the reactor with porous anode and plate cathode operating at a cell voltage of 3.0 V, an electrolyte flow rate of 10^{-6} m^3 s^{-1} and an inlet NaCl concentration of 100 mol m^{-3}

current density (j_a), and Fig. 10 shows the corresponding predicted reversible potentials of Cl_2 evolution (E_{Cl_2/Cl^-} (SHE)), O_2 evolution (E_{O_2/H_2O} (SHE)), and the overpotentials ($\eta_{Cl_2} = \Phi_a - \phi - E_{Cl_2/Cl^-}$) and ($\eta_{O_2} = \Phi_a - \phi - E_{O_2/H_2O}$), along the height of the anode, for the reactor with plate electrodes operating at a cell voltage of 3.0 V, an electrolyte flow rate of 10^{-6} m^3 s^{-1} and an inlet NaCl concentration of 100 mol m^{-3}.

The ratio of $Cl_{2(aq)}$ to Cl^- concentration increased with height of the reactor and so the reversible potential of the electro-oxidation of Cl^- also increased from 1.38 V (SHE) at the reactor inlet to 1.46 V (SHE) at the reactor outlet. Although the resulting overpotential increased slightly by 0.015 V, current densities for Cl^- oxidation decreased from 215 A m^{-2} at the inlet to 185 A m^{-2} at the outlet due to the decrease in Cl^- concentrations.

The increase in H^+ concentration produced by O_2 evolution at the anode was predicted to have little effect on the reversible potential for O_2 evolution; being kinetically controlled and as its overpotential increased by 0.09 V from the inlet to the outlet of the reactor, its current density increased from negligible to 30 A m^{-2}.

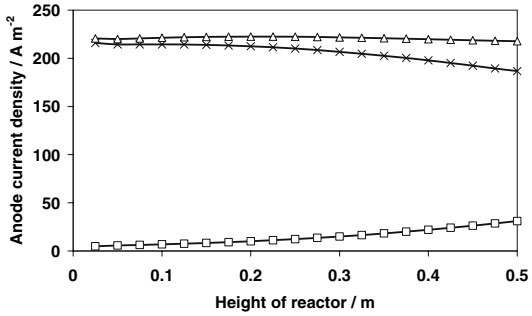

Fig. 9 Predicted current density profiles of Cl^- oxidation (j_{Cl2}) (×), O_2 evolution (j_{O2}) (□) and total anode current density (Δ), along the height of the anode, at a cell voltage of 3.0 V, an electrolyte flow rate of 10^{-6} m^3 s^{-1} and an inlet NaCl concentration of 100 mol m^{-3}, for the reactor with plate electrodes

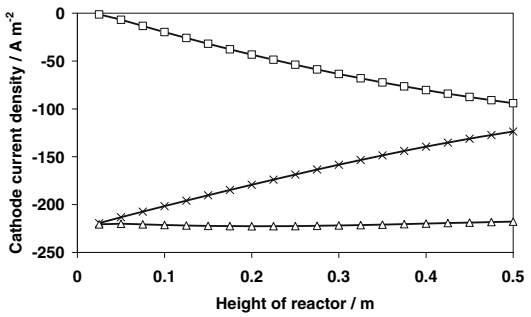

Fig. 11 Predicted current density profiles of H_2 evolution (j_{H2}) (×), reduction of OCl^- (j_{ClO}) (□) and total cathode current density (Δ), along the height of cathode, at a cell voltage (U_{cell}) of 3.0 V, an electrolyte flow rate of 10^{-6} m^3 s^{-1} and an inlet NaCl concentration of 100 mol m^{-3}, for the reactor with plate electrodes

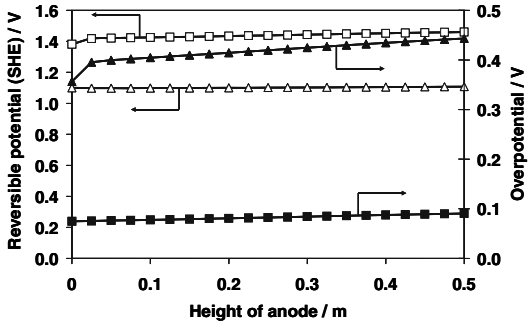

Fig. 10 Predicted reversible potentials of Cl_2 evolution (E_{Cl_2/Cl^-} (SHE)) (□), O_2 evolution (E_{O_2/H_2O} (SHE)) (Δ), and the overpotentials ($\eta_{Cl_2} = \Phi_a - \phi - E_{Cl_2/Cl^-}$) (■) and ($\eta_{O_2} = \Phi_a - \phi - E_{O_2/H_2O}$) (▲), at the surface of anode, along the height of anode, at a cell voltage of 3.0 V, an electrolyte flow rate of 10^{-6} m^3 s^{-1} and an inlet NaCl concentration of 100 mol m^{-3}, for the reactor with parallel plate electrodes

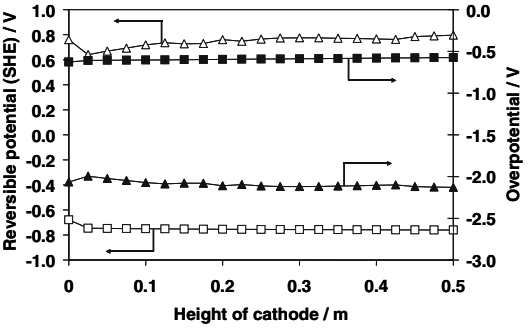

Fig. 12 Predicted reversible potential of H_2 evolution (E_{H_2O/H_2} (SHE)) (□), reduction of OCl^- (E_{ClO^-/OH^-} (SHE)) (Δ), and the overpotentials ($\eta_{H_2} = \Phi_c - \phi - E_{H_2O/H_2}$) (■) and ($\eta_{ClO^-} = \Phi_c - \phi - E_{ClO^-/OH^-}$) (▲), at the surface of cathode, along the height of cathode, at a cell voltage of 3.0 V, an electrolyte flow rate of 10^{-6} m^3 s^{-1} and an inlet NaCl concentration of 100 mol m^{-3}, for the reactor with parallel plate electrodes

Figure 11 shows the predicted current density profiles of H_2 evolution (j_{H_2}), reduction of OCl^- (j_{OCl^-}) and total cathode current density. Figure 12 shows the corresponding predicted reversible potential of H_2 evolution (E_{H_2O/H_2} (SHE)), reduction of OCl^- (E_{ClO^-/OH^-} (SHE)), and the overpotentials ($\eta_{H_2} = \Phi_c - \phi - E_{H_2O/H_2}$) and ($\eta_{ClO^-} = \Phi_c - \phi - E_{ClO^-/OH^-}$), along the height of the cathode, for the reactor with plate electrodes operating at a cell voltage of 3.0 V, an electrolyte flow rate of 10^{-6} m^3 s^{-1} and an inlet NaCl concentration of 100 mol m^{-3}.

Neglecting the decrease in the reversible potential of H_2 evolution close to the entrance of the reactor, caused by the significant increase in OH^- concentration, the variation in both reversible potential and overpotential for H_2 evolution appeared to be insignificant. The absolute overpotential decreased by only 0.015 V between the inlet and outlet of the reactor. However, as H_2 evolution was under kinetic control and its current density decreased exponentially with overpotential and, combined with fast kinetics (an exchange current density of 0.01 A m^{-2} and a Tafel slope of 140 mV decade^{-1}), the absolute current density of H_2 evolution decreased from −220 A m^{-2} at the inlet of the reactor to −124 A m^{-2} at the outlet of the reactor.

The reversible potential of the reduction of OCl^- was predicted to have a positive value of 0.8 V (SHE), resulting in a very large absolute overpotential ($\eta_{OCl^-} = -2$ V). Therefore, its current density was under total mass transport control and increased with the reactor height, from negligible at the inlet, to −94 A m^{-2} at the outlet, as the OCl^- concentration, produced by the hydrolysis of HOCl, increased.

In practice the total current density is expected to decrease along the electrode due to the accumulation of bubbles with reactor height. Accumulation of bubbles decreases the effective conductivity of the electrolyte and increases the ohmic potential drop within the bulk electrolyte. As the cell voltage is fixed, an increase in ohmic loss of potential in the bulk electrolyte leads to a decrease

in the overpotential for electrochemical reactions, so decreasing current densities.

The fraction of anodic current lost to O_2 evolution ($j_{O_2}/(j_{Cl_2}+j_{O_2})$) and the fraction of cathodic current lost as the reduction of OCl^- ($j_{OCl^-}/(j_{H_2}+j_{OCl^-})$) both increased with the reactor height, as implied by the partial current density data in Figs. 9 and 11, respectively. The overall hypochlorite current efficiency ($\Phi_{overall}$), defined as:

$$\Phi_{overall} = 1 - j_{O_2}/(j_{Cl_2}+j_{O_2}) - j_{OCl^-}/(j_{H_2}+j_{OCl^-}) \qquad (70)$$

would also decrease with increase in the height. Therefore, increasing the reactor height to increase single-pass conversion of Cl^- would not be favourable.

Figures 13 and 14 show the predicted partial current density profiles of Cl_2 evolution (j_{Cl_2}) and O_2 evolution (j_{O_2}) within the porous anode, respectively, and Figure 15 shows the predicted partial current densities for H_2 evolution (j_{H_2}) and reduction of OCl^- ions (j_{OCl^-}), and the fraction of cathode current lost to the reduction of OCl^-, along the cathode; for the reactor with a porous anode and plate cathode operating at a cell voltage of 3.0 V, an electrolyte flow rate of 10^{-6} m^3 s^{-1} and an inlet NaCl concentration of 100 mol m^{-3}.

The current density for oxidation of Cl^- ions was predicted to have the same profile as that for Cl^- concentrations, as explained earlier in this section. The current density for O_2 evolution increased from the feeder anode towards the bulk electrolyte. Due to high electronic conductivity of the porous anode, the potential drop within the solid phase was negligible. As the distance from feeder anode increased, current was transferred from the solid to the liquid phase and the liquid phase potential decreased. Since the equilibrium potential for O_2 evolution was approximately constant within the porous anode, its overpotential and hence, current density increased with distance from the feeder anode.

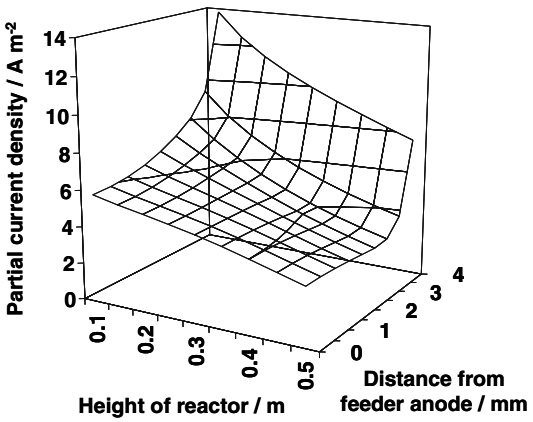

Fig. 13 Predicted partial current density of Cl_2 evolution within the porous anode, at a cell voltage of 3.0 V, an electrolyte flow rate of 10^{-6} m^3 s^{-1} and an inlet NaCl concentration of 100 mol m^{-3}, for the reactor with porous anode and plate cathode

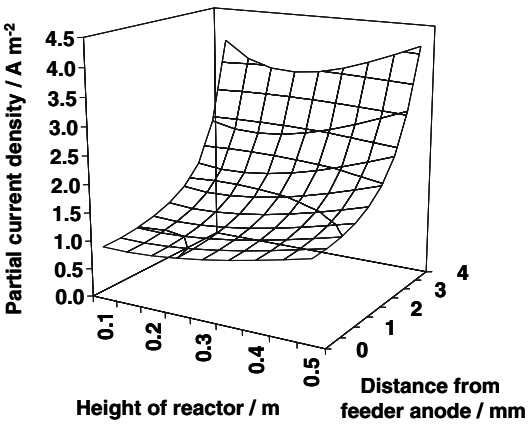

Fig. 14 Predicted partial current density of O_2 evolution within the porous anode, at a cell voltage of 3.0 V, an electrolyte flow rate of 10^{-6} m^3 s^{-1} and an inlet NaCl concentration of 100 mol m^{-3}, for the reactor with porous anode and plate cathode

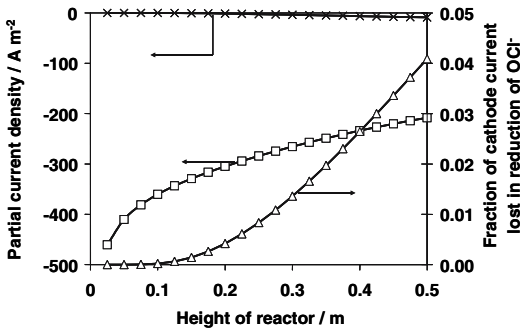

Fig. 15 Predicted partial current densities for H_2 evolution (□) and reduction of OCl^- ions (×), and the fraction of cathode current lost to the reduction of OCl^- (Δ), at a cell voltage of 3.0 V, an electrolyte flow rate of 10^{-6} m^3 s^{-1} and an inlet NaCl concentration of 100 mol m^{-3}, for the reactor with porous anode and plate cathode

The fraction of anodic current lost to O_2 evolution increased from the inlet to the outlet of the reactor. For higher operating cell voltages, at which Cl^- oxidation is under total mass transport control, the anodic current efficiency will also decrease from the feeder anode towards the porous anode/bulk electrolyte interface. As a result, increasing the thickness of the porous anode would increase Cl^- conversion but it would also decrease current efficiency.

At the plate cathode, the current density for H_2 evolution decreased as the reactor height increased, while current densities for reduction of OCl^- ions increased, but to values insignificant compared with those for H_2 evolution.

The predicted fraction of cathodic current lost to reduction of OCl^- ions for the reactor with a porous anode and plate cathode was much lower than that predicted for

the reactor with parallel plate electrodes, similar to the case where a decreased area cathode was used [1,6].

4.3 Conversion and current efficiencies

Figures 16 and 17 compare the performance of the two types of reactor. In order to compare the Cl^- conversion (and the amount of Cl^- converted) predicted by the two models directly, the volumetric flow rate of electrolyte, instead of linear velocity, was used. Due to the difference in geometries between the two reactors, the linear velocity in the reactor with planar anode was five times greater than that for the reactor with the porous anode.

Figure 16 shows the predicted effects of cell voltage on Cl^- conversions for plate anode and porous anode, and overall current efficiencies for plate anode and porous anode, at an electrolyte flow rate of 10^{-6} m^3 s^{-1} and an inlet NaCl concentration of 100 mol m^{-3}. Higher Cl^- conversions were achieved for the reactor with the porous anode, at cell voltages between 2.8 and 3.4 V. For the reactor with the porous anode, total mass transport for the electro-oxidation of Cl^- was also achieved at lower cell voltages, partly due to the lower linear velocity, and partly due to the increase in overpotential across the thickness of the porous anode. For cell voltages $\leq$ 3.0 V, for which the rate of O_2 evolution was less significant, the reactor with the porous anode was predicted to have higher overall current efficiencies than the reactor with a plate anode. Due to a higher surface area for both Cl^- oxidation and O_2 evolution, combined with the increase in overpotential within the thickness of the porous anode, at cell voltages >3.0 V, that reactor was predicted to have lower overall current efficiencies than those for the reactor with a plate anode. For the reactor with a porous anode with an electrolyte flow rate of 10^{-6} m^3 s^{-1}, it was favourable to operate at a cell voltage of 3.0 V, as both Cl^- conversions

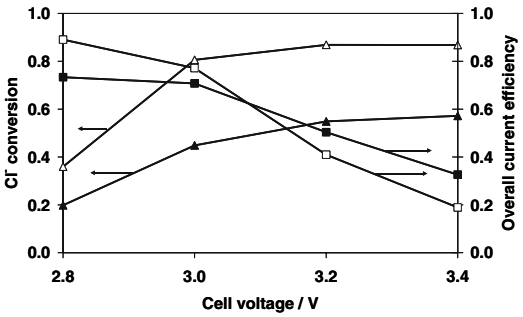

Fig. 16 Predicted effects of cell voltage on Cl^- conversions for plate anode (▲) and porous anode (Δ), and overall current efficiencies for plate anode (■) and porous anode (□), at an electrolyte flow rate of 10^{-6} m^3 s^{-1} and an inlet NaCl concentration of 100 mol m^{-3}

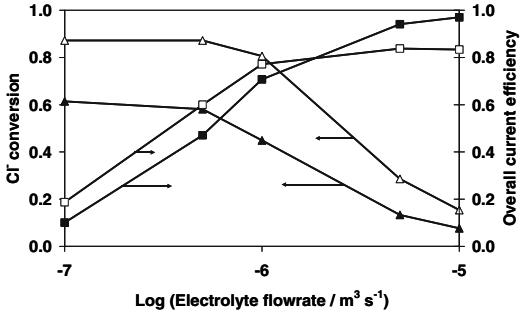

Fig. 17 Predicted effects of electrolyte flow rate on Cl^- conversions for plate anode (▲) and porous anode (Δ), and overall current efficiencies for plate anode (■) and porous anode (□), at a cell voltage of 3.0 V and an inlet NaCl concentration of 100 mol m^{-3}

and overall current efficiencies were greater than those for the reactor with the plate anode.

Figure 17 shows the predicted effects of electrolyte flow rate on Cl^- conversions for plate anode and porous anode, and overall current efficiencies for plate anode and porous anode, at a cell voltage of 3.0 V and an inlet NaCl concentration of 100 mol m^{-3}. At electrolyte flow rates >10^{-6} m^3 s^{-1}, the reactor with the plate anode was predicted to have higher overall current efficiencies, and the opposite was predicted for electrolyte flow rates $\leq$ 10^{-6} m^3 s^{-1}. As a result, the optimal operating conditions for the reactor with the porous anode were a cell voltage of 3.0 V and an electrolyte flow rate of 10^{-6} m^3 s^{-1}, for which high Cl^- conversion (0.81) and high overall current efficiency (0.77) were predicted to be achievable.

4.4 Sensitivity analysis of exchange current density for Cl^- oxidation

As experimental data for the dependence of the exchange current density for Cl^- oxidation ($j_{Cl_2,0}$) on Cl^- concentration could not be found in the literature, a sensitivity analysis of the effect of that exchange current density was carried out by decreasing its value from 1 to 0.1 A m^{-2}. Figure 18 shows the predicted current densities, Cl^- concentrations at the surface of the anode, conversions and the overall current efficiencies with the two different exchange current densities for the reactor with plate electrodes, operating at cell voltages of (a) 3.0 V and (b) 3.2 V, an electrolyte flow rate of 10^{-6} m^3 s^{-1} and an inlet NaCl concentration of 100 mol m^{-3}. For cell voltages $\leq$ 3.0 V, Cl^- oxidation was under mixed kinetic and mass transport control. A lower value of exchange current density decreased current densities, conversions and overall current efficiencies. However, for cell voltages >3.0 V, Cl^- oxidation was under total mass transport control for anode heights >0.2 m, so decreasing the exchange current density

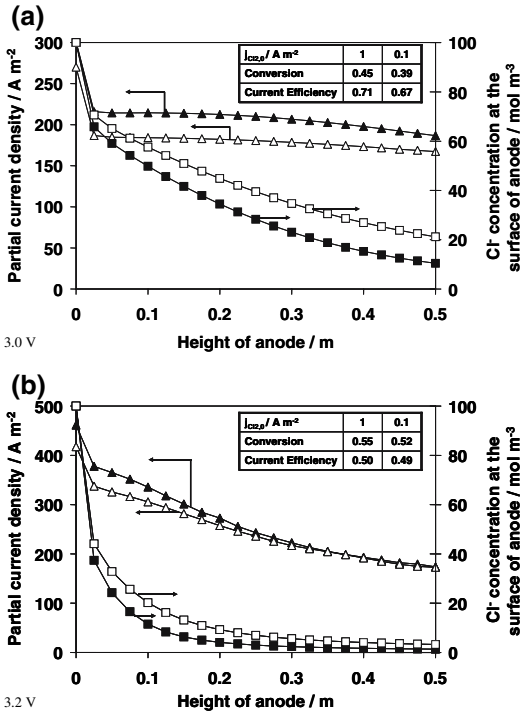

Fig. 18 Predicted effects of exchange current density ($j_{Cl_2,0}$) on partial current densities for Cl^- oxidation (j_{Cl_2}) (▲) and Cl^- concentration at the surface of anode (■) for $j_{Cl_2,0} = 1\,A\,m^{-2}$; and j_{Cl_2} (Δ) and Cl^- concentration (□) for $j_{Cl_2,0} = 0.1 Am^{-2}$, at a cell voltage (U_{cell}) of (**a**) 3.0 V and (**b**) 3.2 V, an electrolyte flow rate of 10^{-6} m^3 s^{-1} and an inlet NaCl concentration of 100 mol m^{-3}, for the reactor with parallel plate electrodes

by an order of magnitude had little effect on current densities, conversions and overall current efficiencies.

5 Conclusions

(a) Pseudo two-dimensional steady-state models were developed for two flow-by reactors for the production of hypochlorite, one with two parallel plate electrodes and the other a 4 mm thick PbO_2-coated graphite felt anode and a plate cathode.

(b) For an electrolyte volumetric flow rate of 10^{-6} m^3 s^{-1}, a cell voltage of 3.0 V and an inlet NaCl of 100 mol m^{-3}, the single-pass conversion of Cl^- was predicted to increase from 0.45 for the reactor with the planar anode to 0.81 for the reactor with the porous anode. For the same operating conditions, the overall current efficiency was also predicted to increase from 0.71 to 0.77 by using the porous anode.

(c) For cell voltages >3.0 V increasing the thickness of the porous anode increased Cl^- conversions, but decreased current efficiencies, due to the potential variation across the porous anode.

(d) The predicted fraction of cathodic current lost to reduction of OCl^- ions for the reactor with a porous anode and plate cathode was much lower than that predicted for the reactor with parallel plate electrodes due to the difference in surface area between the porous anode and the plate cathode.

Acknowledgement The authors thank the UK Engineering and Physical Sciences Research Council for a studentship for Chun-yee Cheng.

References

1. Ibl N, Vogt H (1983) In: Yeager E (ed) Comprehensive treatise of electrochemistry, vol 2. Plenum, New York
2. Czarnetzki LR (1989) Aspects of electrochemical production of hypochlorite and chlorate. PhD Thesis, Technische Universiteit Eindhoven, Holland
3. Byrne P, Fontes E, Parhammar O, Lindbergh G (2001) J Electrochem Soc 148(10):D125
4. Ibl N, Landolt D (1968) J Electrochem Soc 115(7):713
5. Landolt D, Ibl N (1970) Electrochim Acta 15:1165
6. Robertson PM, Gnehm W, Ponto L (1983) J Appl Electrochem 13:307
7. Hammar L, Wranglén G (1964) Electrochim Acta 9:1
8. Rudolf M, Roušar I, Krýsa J (1995) Electrochim Acta 40(2):169
9. Cheng CY, Kelsall GH, Pilone D (2005) J Appl Electrochem 35:1191
10. Boxall C, Kelsall GH (1992) IChem E Symp Series IChemE, Rugby, UK 127:59
11. Gijsbers HFM, Janssen LJJ (1989) J Appl Electrochem 19(5):637
12. Leah RT (2001) Computer simulations and experimental studies for chlor-alkali electrochemical cells. PhD Thesis, University of London
13. Cornell A (2002) Electrode reactions in the chlorate process. PhD Thesis, Royal Institute of Technology, Stockholm
14. Appleby AJ, Chemla M, Kita H, Bronoël G (1973) In: Bard AJ (ed) Encyclopaedia of electrochemistry of the elements IXa-3. Marcel Dekker, New York, p 524
15. Spalding CW (1962) AIChE J 8(5):685
16. Wang TX, Margerum DW (1994) Inorg Chem 33:1050
17. Renard JJ, Bolker HI (1976) Chem Rev 76(4):487
18. Ibl N, Vogt H (1983) In: Yeager E (ed) Comprehensive treatise of electrochemistry, vol 6. Plenum, New York
19. Czarnetzki LR, Janssen LJJ (1992) J Appl Electrochem 22:315
20. Bard AJ, Parsons R, Jordan J (1985) Standard potentials in aqueous solution. Marcel Dekker, New York
21. Newman JS (1991) Electrochemical systems, 2nd edn. Prentice Hall, Englewood Cliffs, p 255
22. Chao MS (1968) J Electrochem Soc 115(11):1172
23. Gonzalez-Garcia J, Bonete P, Exposito E, Montiel V, Aldaz A, Torregrosa-Macia R (1999) J Mater Chem 9:419
24. Carta R, Palmas S, Polcaro AM, Tola G (1991) J Appl Electrochem 21(9):793